Monoclinic high-pressure polymorph of AlOOH predicted from first principles

Xin Zhong,[1,2,3] Andreas Hermann,[4] Yanchao Wang,[2,*] and Yanming Ma[2,3,†]

[1]*Key Laboratory of Functional Materials Physics and Chemistry of the Ministry of Education,*
Jilin Normal University, Siping 136000, China
[2]*State Key Laboratory of Superhard Materials, Jilin University, Changchun 130012, China*
[3]*Beijing Computational Science Research Center, Beijing 10084, China*
[4]*Centre for Science at Extreme Conditions and SUPA, School of Physics and Astronomy,*
The University of Edinburgh, Edinburgh EH9 3FD, United Kingdom

Aluminum oxide hydroxide, AlOOH, is a prototypical hydrous mineral in the geonomy. The study of the high-pressure phase evolution of AlOOH is of fundamental importance in helping to understand the role of hydrous minerals in the water storage and transport in Earth, as in other planets. Here, we have systematically investigated the high-pressure phase diagram of AlOOH up to 550 GPa using the efficient crystal structure analysis by particle swarm optimization (CALYPSO) algorithm in conjunction with first principles calculations. We predict a peculiar monoclinic phase (space group $P2_1/c$, 16 atoms/cell, $Z = 4$) as the most stable phase for AlOOH above 340 GPa. The occurrence of this new phase results in the breakup of symmetric linear O-H-O hydrogen bonds into asymmetric, bent O-H-O linkages and in sevenfold coordinated metal cations. The new $P2_1/c$ phase turns out to be a universal high-pressure phase in group 13 oxide hydroxides, and stable for both compressed GaOOH and InOOH. The formation of the new phase in all compounds is favored by volume reduction due to denser packing.

I. INTRODUCTION

The processes by which volatiles such as water, carbon, or nitrogen are cycled between Earth's surface layers and mantle are crucial to our understanding of the surface environment [1,2]. Earth's atmosphere and oceans are believed to be exhalations from the mantle [3]. Conversely, the presence of volatiles in Earth's interior affects its properties drastically, for instance, to lower the melting temperature of the mantle, transport elements in fluids, enhance diffusion and creep, and possibly change the location of the core-mantle boundary [4]. It has therefore been a long-standing question to explore the high-pressure behavior of water in Earth's deep mantle. At high-pressure and high-temperature conditions, water usually exists in the form of OH^- anions and is stored in hydrous or nominally anhydrous minerals [5,6]. Thus, the phase transformation and the properties of high-pressure hydrous minerals have attracted considerable petrologic and geophysical interest. Recently, the first evidence for natural ringwoodite, a high-pressure form of the mineral olivine, with a water content of up to 1%, has raised the possibility of large water reservoirs in the mantle transition zone [7,8]. As we know, the pressure in the mantle and cores of Jupiter, Saturn, Uranus, and Neptune are assumed to be much higher than that of Earth [9]. It is thus worthwhile to investigate the ultra-high-pressure properties of known hydrous minerals, being as they are of great important for our understanding of the physics and chemistry of planetary interiors. However, the conditions occurring in the mantle and cores are not easily accessible to experiment, and *ab initio* simulations are helpful to explore the states of matter under such extreme conditions as those found in giant rocky planets.

The main sources of hydrous minerals are thought to be hydrated magnesium and aluminum silicates, i.e., phases within the (MgO/Al_2O_3)-SiO_2-H_2O systems. The former feature a variety of true ternary phases [10] and are assumed to be important water carriers in peridotitic parts of subducting slabs. Among the latter, several aluminum-rich ternary phases have been synthesized, among them the so-called phase Egg, $AlSiO_3OH$ [11–14]. Recent x-ray diffraction papers at high pressure and high temperature have shown that phase Egg decomposes into δ aluminum oxide hydroxide (δ-AlOOH) and stishovite SiO_2 at 23 GPa and 1000 °C [15]. This decomposition reaction suggests that water stored in phase Egg can be carried further into the mantle by δ-AlOOH. In our current understanding, among the numerous known hydrous minerals, only δ-AlOOH and the hydrous magnesium silicate phase D ($MgSi_2O_6H_2$) are stable above 20 GPa [16,17], which corresponds to the conditions in Earth's lower mantle. Pressure-induced hydrogen bond symmetrization occurs in those two phases above approximately 30 and 40 GPa, respectively [18,19]. A recent theoretical prediction and subsequent experimental verification have shown that phase D undergoes a phase transition to a new high-pressure hydrous phase (phase H, $MgSiO_4H_2$) plus stishovite $\sim$40 GPa. This new phase is stable at least up to 50 GPa and could be stabilized further by dissolution of δ-AlOOH [20]. It is then even more pertinent to study the high-pressure properties of the latter.

The δ phase of aluminum hydroxide oxide (space group 31, $P2_1nm$) is a high-pressure phase of α-AlOOH (diaspore, space group 62, $Pbnm$) and γ-AlOOH (boehmite, space group 63, $Cmcm$) and can be synthesized $\sim$21 GPa and 1000 °C [21]. Although a few papers have shown that hydrous materials commonly dissociate and release H_2O under pressures of a few

---
*Corresponding author: wyc@calypso.cn
†Corresponding author: mym@jlu.edu.cn

tens of gigapascals [22], high-pressure experiments reported that δ-AlOOH continues to exist up to $\sim$134 GPa [23].

Recent first principles density functional calculations suggested a cubic pyrite-type AlOOH phase (space group 205, Pa-3) with symmetric hydrogen bonds to be stable above 170 GPa. Eventually, a decomposition of AlOOH into aluminum oxide and water is expected, following the reaction $2*\text{AlOOH} \rightarrow \text{Al}_2\text{O}_3 + \text{H}_2\text{O}$. The dissociation of pyrite-type AlOOH into a CaIrO$_3$-type phase of Al$_2$O$_3$ plus ice X was predicted to occur at a pressure of 300 GPa [24]. There is no doubt that AlOOH has an unexpectedly wide stability range in pressure when compared to other hydrous materials.

Aluminum oxide hydroxide has a high-pressure phase evolution similar to its group 13 homologues GaOOH and InOOH, and conversely, both GaOOH and InOOH can be expected to behave as low-pressure analogues of AlOOH. At ambient conditions, both α-GaOOH and InOOH crystallize in the α-AlOOH structure type with space group $Pbnm$ [25]. With increasing pressure, the α-GaOOH structure transforms to an orthorhombic structure with space group $P2_1nm$, which is the typical δ phase-structure type of AlOOH [26], and the CaCl$_2$-type structure of InOOH is isostructural to δ-AlOOH. Finally, the pyrite type of InOOH is also comparable to AlOOH at high pressure. This is not surprising: Al^{3+} is a lighter homologue of both Ga^{3+} and In^{3+}, and the pressure-homologue rule suggests that phase transitions in the larger cation phase occur at lower pressures than in the small cation phase [27]. Through high-pressure and high-temperature x-ray diffraction experiments, the pyrite type of InOOH was successfully synthesized $\sim$14 GPa and 1300 K [28]. Thus, as far as we know, AlOOH, GaOOH, and InOOH follow the same structural sequence $Pbnm \rightarrow P2_1nm \rightarrow Pa$-3, where only GaOOH-$Pa$-3 has not been observed yet. Previous papers also reported that the dehydration of InOOH into In$_2$O$_3$ + H$_2$O is unlikely to occur at least up to 50 GPa under static conditions [29]. The transition pressures in both GaOOH and InOOH are lower than those in AlOOH; therefore, if a new phase of AlOOH was found, it would form a likely candidate for new high-pressure phases in both GaOOH and InOOH.

There is a possibility that some unknown structures are energetically stable beyond the dehydration stage of AlOOH and InOOH. These uncertainties have impeded an in-depth understanding and further exploration of the structural sequence and stability limit of both minerals. Thus, it is greatly desirable for us to explore the stability limit and the dissociation reaction of the hydrous phases of AlOOH and InOOH.

Here, we present an extensive structure search to uncover the high-pressure structures of AlOOH, GaOOH, and In-OOH using the crystal structure analysis by particle swarm optimization (CALYPSO) method [30,31]. The effectiveness of our structure searching method has been demonstrated by recent successes in predicting high-pressure structures of various compounds [32–37]. Our paper confirmed the transition sequence of AlOOH, and we have identified a new stable monoclinic $P2_1/c$ phase for AlOOH. This new phase is energetically superior to the previously proposed pyrite-type AlOOH at very high pressures. While it is metastable with respect to decomposition into Al$_2$O$_3$ and ice, this new phase is stable as a high-pressure phase in both GaOOH and InOOH and pushes the onset of dehydration of

InOOH into In$_2$O$_3$ + H$_2$O $-$ VIII at least up to 80 GPa, while preventing dehydration of GaOOH at least up to 260 GPa. Our present paper improves the current understanding of the high-pressure evolution of AlOOH and the group 13 oxide hydroxides in general, and it represents a significant step toward understanding the behavior of hydrous compounds under extreme conditions.

II. CALCULATION METHODS AND STRUCTURE MODELS

We obtain candidate structures of AlOOH at external high pressures by using swarm-intelligence CALYPSO structure searching simulations [30,31] unbiased by any prior known structure knowledge and in conjunction with first principles density functional calculations. The remarkable feature of this methodology is the capability of predicting a stable structure with only the knowledge of the chemical composition under given external conditions (for example, pressure).

We searched for structures of AlOOH with simulation cell sizes of 1–4 formula units (f.u.) at pressures of 100, 150, 200, 250, 300, 350, 400, 500, and 550 GPa using the CALYPSO package [30,31]. The local structural relaxations calculations were performed in the framework of density functional theory, using the generalized gradient approximation, to model electronic exchange-correlation effects, and the frozen-core projector-augmented wave (PAW) method [38,39], as implemented in the Vienna *Ab initio* Simulation Package (VASP) code [40,41]. Applying the local density approximation (LDA) to the exchange-correlation energy often results in severely overestimating hydrogen-bonded interactions [42], but for comparison, we present LDA results in the Supplemental Material [43]. The PAW potentials were used to describe the ionic core potentials of Al($3s^2 3p^1 3d^0$), Ga($3d^{10} 4s^2 4p$ [1]), In($4d^{10} 5s^2 5p$ [1]), O($2s^2 2p$ [4]), and H ($1s$ [1]), respectively, with cutoff radii of 1.9, 2.6, 3.1, 1.52, and 1.1 Bohrs, respectively. A cutoff energy of 520 eV for the expansion of the wave function into plane waves and appropriate regular Monkhorst-Pack (MP) [44] k-point grids were chosen to ensure that all enthalpy calculations were well converged to 1 meV/atom. The accuracy of the total energies obtained within the framework of density functional theory is in many cases sufficient to predict the stability of structures. Phonon calculations of the $P2_1/c$ phase were carried out using a supercell approach as implemented in the Phonopy package, using a $2 \times 2 \times 2$ supercell [45].

III. RESULTS AND DISCUSSION

A. Aluminum oxide hydroxide

Our structure searches on AlOOH, solely using the desired chemical compositions of Al:O:H = 1:2:1, readily reproduced the previously known δ-AlOOH (space group 58, $Pnnm$) at $P = 100$ and 150 GPa and the pyrite-type (space group 205, Pa-3) structures at 200, 250, 300, and 350 GPa. This confirmed the reliability of our prediction method as applied to the AlOOH system. Both the δ-AlOOH and the pyrite phase feature symmetric, linear hydrogen bonds (the symmetrization of which leads to space group changes from $P2_1nm$ to $Pnnm$ and from $P2_13$ to Pa-3), with oxygen-hydrogen bond
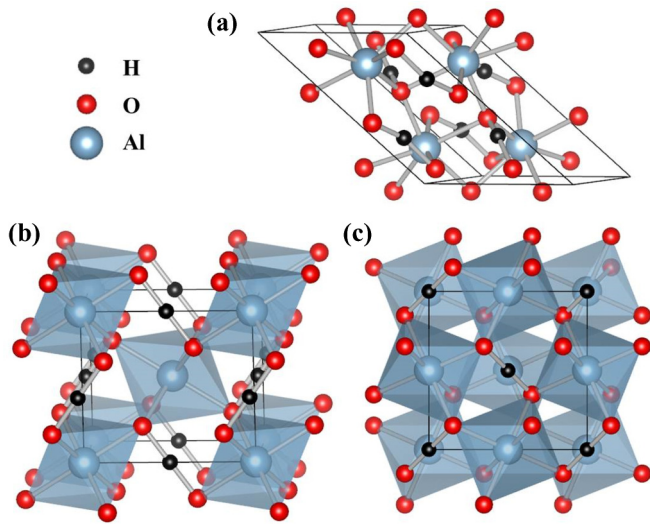
FIG. 1. Crystal structures of the (a) $P2_1/c$ phase of AlOOH, (b) δ-AlOOH, and (c) pyrite-type AlOOH. The blue, red, and black spheres represent aluminum, oxygen, and hydrogen atoms, respectively.

distances ($R_{O\text{-}H}$) of about 1.120 and 1.097 Å, respectively, at 160 and 200 GPa [Fig. 1(b) and 1(c)]. At elevated pressures of 400, 500, and 550 GPa, our structure predictions uncovered a peculiar monoclinic phase (space group 14, $P2_1/c$, $Z = 4$, 16 atoms/cell), as depicted in Fig. 1(a). This primitive monoclinic structure has lattice parameters of $a = 5.5928$ Å, $b = 4.0590$ Å, $c = 3.8306$ Å, and $\beta = 139.51°$ at 500 GPa. In this structure, the hydrogen bonds revert to an asymmetric motif and deviate from a linear arrangement: the $O_1\text{-}H\text{-}O_2$ angle is 156.0°, and the two H-O bond lengths are $R_{O1\text{-}H} = 1.118$ Å and $R_{O2\text{-}H} = 1.013$ Å, all at 500 GPa. Each aluminum atom is sevenfold coordinated to oxygen atoms [Fig. 1(a)], with the nearest-neighbor Al-O separations ranging from 1.593 to 1.719 Å at 500 GPa. Conversely, half of the oxygen atoms are fourfold coordinated to aluminum atoms. In contrast, in the pyrite phase, each aluminum atom

is sixfold coordinated to oxygen, and the nearest-neighbor Al-O separations are identical (1.647 Å) at 500 GPa. Thus, pressure induces the trend of increasing coordination number of both aluminum and oxygen atoms in AlOOH, as could be expected, but the $P2_1/c$ phase (with edge-sharing AlO_7 polyhedra) represents a nontrivial departure from the pyrite type (with distorted corner-sharing AlO_6 octahedra).

Figure 2(a) shows the energetic trend toward hydrogen bond symmetrization at low pressures and, on the right, the calculated static enthalpies of all high-pressure structures relative to pyrite-type AlOOH as a function of pressure. In the papers by Tsuchiya *et al.*, pressure-induced hydrogen bond symmetrization of both δ-AlOOH and the pyrite phase were reported to occur at P of $\sim$30 and 15 GPa [19,46], respectively, which was determined by the continuous displacement of hydrogen atoms from the asymmetric off-centered position between two neighboring oxygen atoms. In our paper, in order to directly observe how the asymmetric hydrogen bonding structures transform to the symmetric hydrogen bonding structures, we compared the enthalpies of these four structures with increasing pressure [Fig. 2(a)]. The formation of symmetric linear hydrogen bonds in orthorhombic δ-AlOOH and cubic pyrite-type AlOOH is energetically favorable around 25–30 GPa and 10–15 GPa, respectively. These results are consistent with the previous calculation. At P of $\sim$172.0 GPa [Fig. 2(b)], we find the pyrite phase becomes more stable than δ-AlOOH, also in agreement with previous calculations [24]. The newly predicted $P2_1/c$ phase of AlOOH then becomes more stable than the pyrite-type phase.

However, at P of $\sim$340 GPa, relevant decomposition reactions must consider high-pressure phases of Al_2O_3 (both the $CarIrO_3$ type and the U_2S_3 type [47]) and of ice (all of ice-X, ice-$Pbcm$, and ice-$Pbca$). The transition pressures of ice-X to ice-$Pbcm$ and ice-$Pbcm$ to ice-$Pbca$ are predicted to be $P = 300$ GPa [48] and $P = 710$ GPa [49], respectively. In our calculations, those phase transitions occur $\sim$305.0 and $\sim$718.5 GPa, respectively, which is consistent with the previous papers. Water's phase diagram is rich, and the $Pbca$ phase of ice is the first structure that features bent (if symmetric)
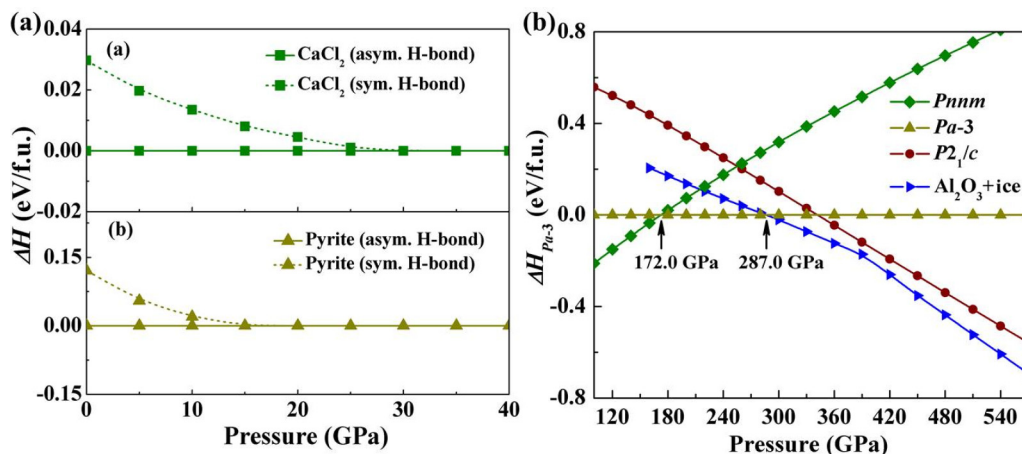
FIG. 2. The calculated static enthalpies of various AlOOH structures. Left: comparing asymmetric and symmetric hydrogen bonding in both δ-AlOOH ($CaCl_2$ structure type) (a) and Pa-3-AlOOH (pyrite structure type) (b). Right: comparing the high-pressure structures relative to δ-AlOOH, as a function of pressure; note the kink in the stability of Al_2O_3 + ice due to a new Al_2O_3 phase at 370 GPa.
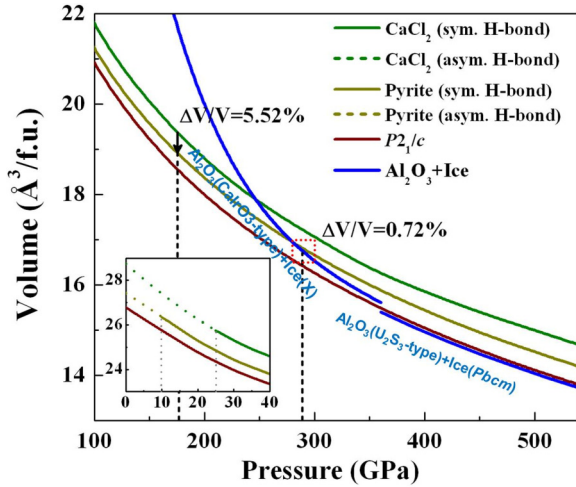
FIG. 3. Equations of state of the CaCl$_2$-, pyrite-, and monoclinic-type phases of AlOOH, as well as Al$_2$O$_3$ + H$_2$O. Solid and dashed lines indicate the symmetric and asymmetric hydrogen bonded structures, respectively. Vertical lines and arrows indicate transition pressures and are labeled with calculated volume collapses. The inserted picture shows the transitions from asymmetric to symmetric hydrogen bonding in both δ-AlOOH (CaCl$_2$ structure type) and pyrite-type AlOOH at low pressure.

hydrogen bonding; the stability range of this phase is 710–780 GPa [50]. Using these phases, we find that at P of ∼295 GPa, calculated ground state enthalpies indicate a dissociation into CaIrO$_3$-type Al$_2$O$_3$ (space group 63, *Cmcm*) and ice (space group 57, *Pbcm*) [Fig. 2(b)]. Even though $P2_1/c$-AlOOH is more stable than the pyrite phase above P of ∼340 GPa, the advent of the U$_2$S$_3$-typeAl$_2$O$_3$ above P of ∼370 GPa [47] means that the dehydration reaction remains favorable in the ground state up to the highest pressures studied here.

Figure 3 shows the equations of state of the $P2_1nm$ and *Pnnm* phases of δ-AlOOH, the $P2_13$ and *Pa*-3 phases of pyrite-type AlOOH, and our newly predicted $P2_1/c$ phase. It is found that the *Pa*-3 phase unit cell volume is smaller than that of the *Pnnm* phase. This phase transition reduces the volume by ∼5.5%. At the transition pressure of the dissociation reaction from the pyrite phase to Al$_2$O$_3$ + ice, the volume reduction is ∼0.7%. At higher pressure, the volume per formula unit of the dissociated phases is slightly smaller than that of the $P2_1/c$ phase. From the viewpoint of theoretical calculation, and not surprisingly, the phase sequence always tends to favor the most compact arrangement. In the $P2_1/c$ phase, hydrogen bonds are neither symmetric nor linear. This is similar to what is seen in pure ice [34,51,52] and is driven by the need to reduce molecular volumes under increasing pressure. A structure that is based on the $P2_1/c$ phase but features linear symmetric hydrogen bonds is, at $P = 400$ GPa, 0.12 eV/f.u. higher in enthalpy than the $P2_1/c$ phase.

The stability of a structure cannot be determined exclusively by comparing enthalpies, since a structure might be subject to dynamic instabilities or, vice versa, be stabilized kinetically. We calculated phonon dispersion curves for the $P2_1/c$ phase of AlOOH at 550 GPa, using the supercell method [53]. The absence of any imaginary phonon frequencies in the
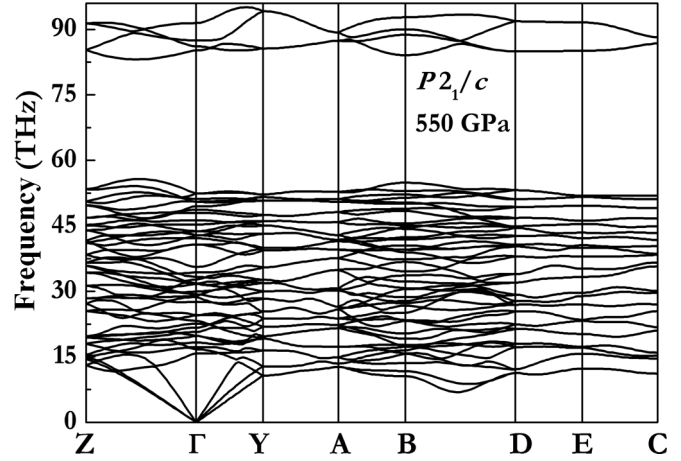
FIG. 4. Phonon dispersions of $P2_1/c$ phase of AlOOH at 550 GPa. These phonon calculations demonstrated the structural stabilities of the predicted $P2_1/c$ phase of AlOOH in view of the absence of any imaginary phonons.

whole Brillouin zone indicates that the $P2_1/c$ structure is dynamically stable (Fig. 4).

We used the phonon densities of state of $P2_1/c$-AlOOH, as well as Pa-3-AlOOH, Al$_2$O$_3$, and ice, to estimate the relative free energies $F(T,V)$ of the phases in the quasiharmonic approximation by considering the vibrational contributions to the entropy. The resultant P-T phase diagram is shown in Fig. 5. The $P2_1/c$ phase of AlOOH is predicted to become stable at very high temperatures and pressures, for instance, above 3500 K at 400 GPa. Those conditions are relevant in the mantle of rocky super-Earths [54,55]. The onset temperature
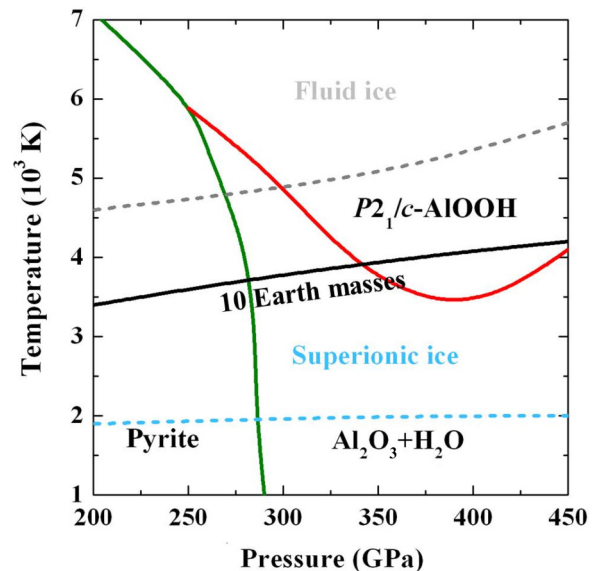
FIG. 5. Finite temperature phase diagram of AlOOH at high pressures. Shown are stability boundaries of the pyrite phase (green line, taken from Ref. [45]) and the $P2_1/c$ phase (red line, our calculations). The black solid line indicates a potential temperature-pressure relation in a rocky super-Earth of 10 Earth masses [53,54]. Gray (blue) dashed lines indicate the onset of ice melting (superionicity) from simulations [55,56].
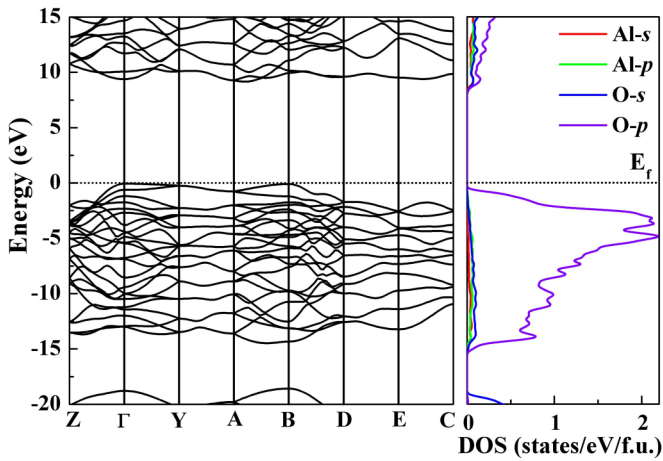
FIG. 6. Calculated electronic band structure (left panel) and DOS (right panel) for the $P2_1/c$ structure of AlOOH at 400 GPa. The dashed black line is an indication of Fermi energy, which is set to zero.

of stability for $P2_1/c$-AlOOH is below estimates of the ice melting line but above the onset of superionicity in ice, as seen in calculations [56,57]. However, while the latter would certainly favor decomposition, it is possible that AlOOH itself forms a superionic phase at those conditions. We find that the covalent O-H bond lengths in $P2_1/c$-AlOOH at 400 GPa are 1.06 Å, slightly longer than those in ice-$Pbcm$ at the same pressure (1.04 Å). This suggests that the covalent O-H bond is weaker in AlOOH than in ice, which would lead to a lower onset temperature of proton mobility, i.e., superionicity, in this phase. This, in turn, could favor the reformation of AlOOH at high temperatures from the constituents in a superionic phase based on the heavy-atom network of the $P2_1/c$ structure.

We then explored the electronic properties of AlOOH under high pressure. To that end, we present the electronic band structure and the density of states (DOS) of the $P2_1/c$ phase at 500 GPa in Fig. 6. This phase is found to be a wide-gap insulator with a direct band gap of ~8 eV at the Γ point. For

comparison, the band gap in δ-AlOOH at $P = 100$ GPa is ~10 eV and in the pyrite-type structure at $P = 300$ GPa is ~12 eV. The upper valence band (UVB) in the $P2_1/c$ phase is dominated by O-2p states. The band width of the UVB is calculated to be a huge 15.2 eV, and it is separated from the lower valence band (LVB) by a gap of ~3 eV. The H-s states are not shown in Fig. 6 because of their small contribution to the UVB, compared to Al and O. The LVB, with a calculated band width of 10 eV, consists of O-2s states and is located −20 to −30 eV below the valence band maximum. The conduction band (CB) is dominated by Al-3d states. The main peak around 14 eV is derived from O-2p and Al-3p antibonding states. Even at very high pressures, AlOOH is a ionic structure, augmented by covalent and some hydrogen bonding. A topological analysis of the electron density confirms this. Partial charges in $P2_1/c$ at $P = 400$ GPa, according to Bader's quantum theory of atoms in molecules (QTAIM analysis [58], are +2.55 and +0.65 for Al and H, and −1.6 for O. Those numbers are basically identical to the charge transfer in both δ-AlOOH and the pyrite-type phase (see the Supplemental Material [43] for more details). An analysis of the electron localization function (ELF) [59] confirms the presence of strong covalent bonds in the system. The ELF has maxima along the nearest Al-O separations, with values from 0.84 to 0.88. The asymmetric O-H-O bonds have ELF maxima of 0.87 (for the shorter O-H separation) and 0.81 (for the longer O-H separation). In the Supplemental Material [43], we show contour plots of the ELF distribution in the unit cell of the $P2_1/c$ phase.

B. Other group 13 oxide hydroxides

As stated earlier, it could be expected that favorable high-pressure phases of AlOOH are also candidates for high-pressure phases of GaOOH and InOOH. With the $P2_1/c$ phase discussed above, this is the case, as it is a stable high-pressure phase for both heavier homologues. For GaOOH, the $P2_1/c$ phase becomes more stable than the pyrite-type structure ~170 GPa [Fig. 7(a)]. There is no tendency for GaOOH to decompose into Ga_2O_3 and ice until at least 260 GPa. For
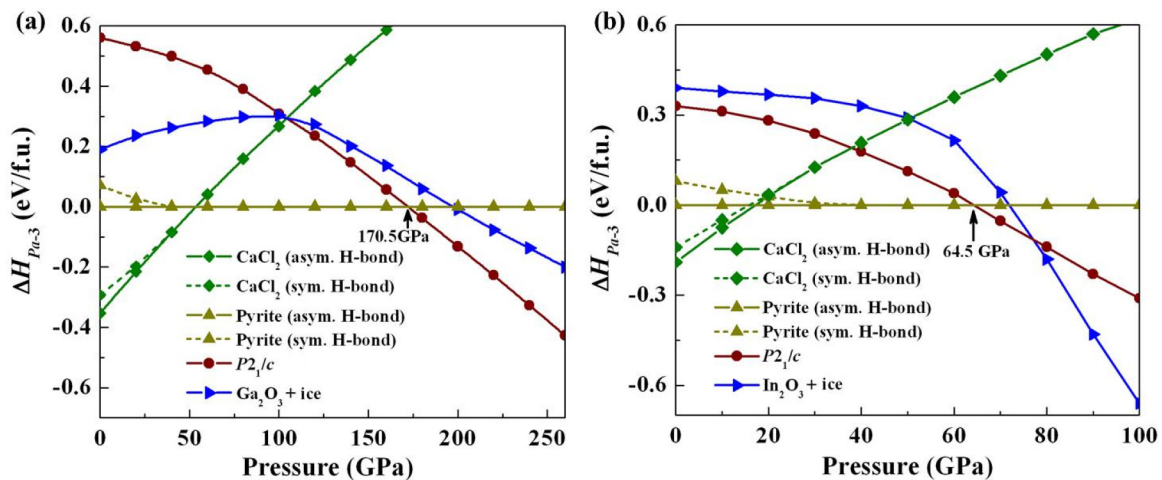
FIG. 7. The calculated static enthalpies of the structures relative to Pa-3 phase of GaOOH (a) and InOOH (b) structure as a function of pressure.
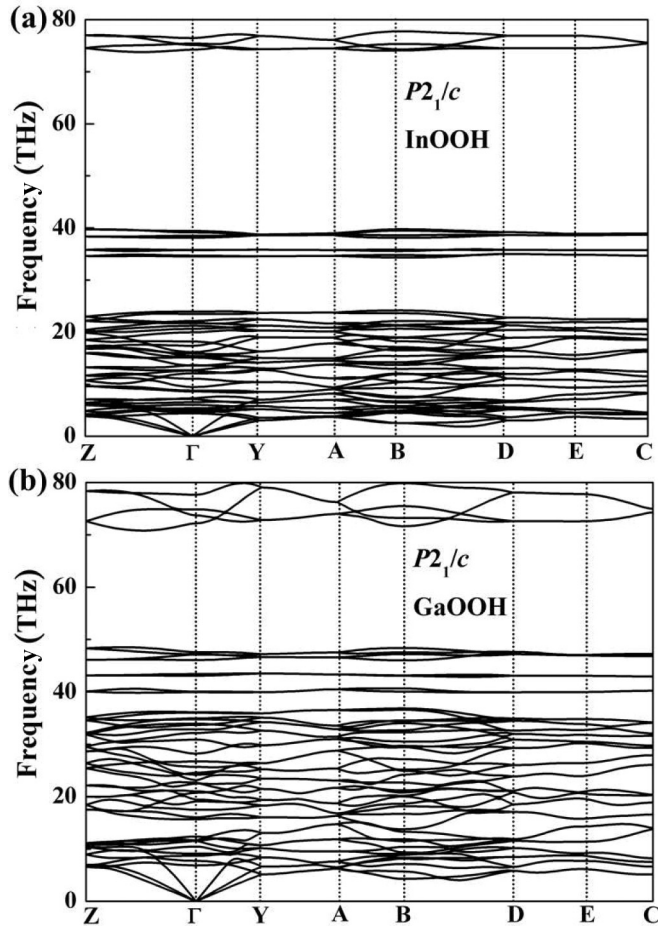
FIG. 8. Phonon dispersions of $P2_1/c$ phase of InOOH at 70 GPa (a) and GaOOH at 200 GPa (b). These phonon calculations demonstrated the structural stabilities of the predicted $P2_1/c$ phase of InOOH and GaOOH in view of the absence of any imaginary phonons.

InOOH [Fig. 7(b)], the $P2_1/c$ phase becomes more stable than the pyrite-type structure at $P = 65$ GPa until, at $P = 77$ GPa, decomposition into In_2O_3 and ice becomes enthalpically favorable. The $P2_1/c$ phase thus extends the stability range of compressed InOOH against decomposition by about 12 GPa and delays dehydration in GaOOH up to very high pressures. In the relevant pressure range, the $P2_1/c$ phases of InOOH and GaOOH are dynamically stable, as the phonon dispersion curves shown later in Fig. 8. Relevant decomposition reactions for both compounds considered high-pressure phases of ice (ice-VIII [60] and ice-X [61]), Ga_2O_3 [Rh_2O_3 (II) type [62] to 160 GPa and the $CaIrO_3$ type [63] for 160–260 GPa], and In_2O_3 [Rh_2O_3 (II) type [62,63] to 40 GPa and Gd_2S_3 type [64] for 40–100 GPa].

Electronically, like AlOOH, both $P2_1/c$-GaOOH and $P2_1/c$-InOOH are wide-gap insulators, albeit with smaller band gaps of 6.5 and 2.5 eV at $P = 200$ and 70 GPa, respectively (Fig. 9). The reduced gaps, compared to AlOOH and in particular for InOOH, are due to lower-lying, unoccupied In-s states; consequently, the ionic character of both GaOOH and InOOH is somewhat less pronounced than that of AlOOH. The Bader partial charges in the $P2_1/c$ phases of GaOOH and InOOH at $P = 200$ and 70 GPa are, respectively, $+2.05$ and
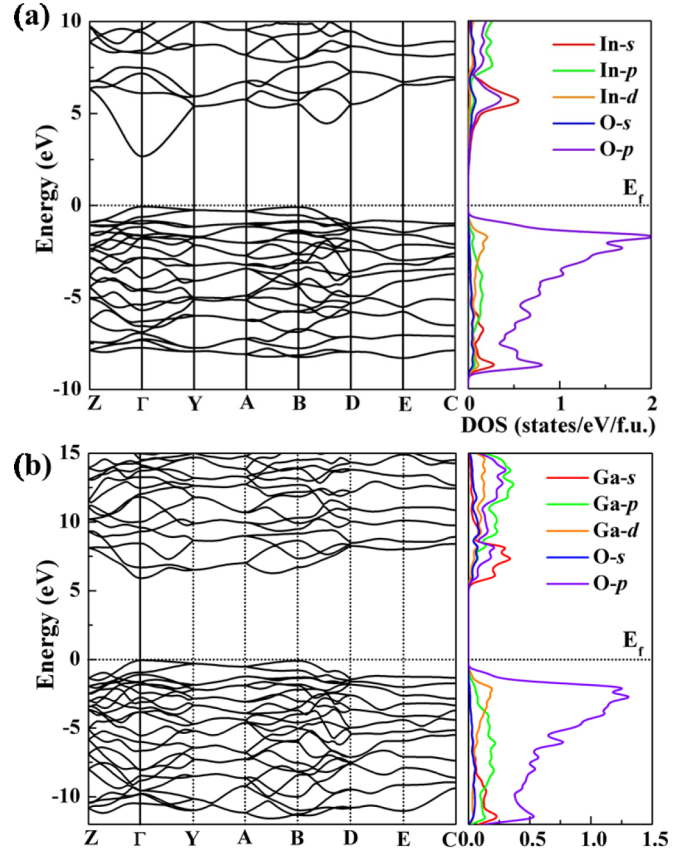
FIG. 9. Calculated electronic band structure (left panel) and DOS (right panel) for the $P2_1/c$ structure of InOOH at 70 GPa (a) and GaOOH at 200 GPa (b). The dashed black line is an indication of Fermi energy, which is set to zero.

$+0.63$ for H and -1.32 for O (Ga) and $+1.95$ and $+0.61$ for H and -1.28 for O (In). As in AlOOH, these numbers are close to both the $CaCl_2$-type and the pyrite-type structure at lower pressures. The stabilization of the $P2_1/c$ phase stems in both compounds from the more compact atomic packing; at the transition pressure, the $P2_1/c$ phase in GaOOH and InOOH, respectively, is more than 3.9% and 3% denser than the pyrite-type phase (Fig. 10).

IV. CONCLUSIONS

To summarize, we have reported new high-pressure phase relations in AlOOH predicted by our swarm intelligence structure simulations. The $P2_1/c$ phase of AlOOH becomes more stable than the pyrite-type structure at 287 GPa but is metastable in the ground state with respect to decomposition into Al_2O_3 and ice up to the highest pressure studied here (about 550 GPa). However, we find this phase, in the quasiharmonic approximation, to be stabilized at very high temperatures, relevant along proposed adiabats of rocky super-Earth planets. A deep-mantle water reservoir in those planets (not available on Earth) could significantly affect their volatile partitioning and their ability to sustain the presence of surface water on geological and evolutionary timescales. Under those extreme conditions (400 GPa, 4000 K), monoclinic AlOOH could conceivably form a superionic
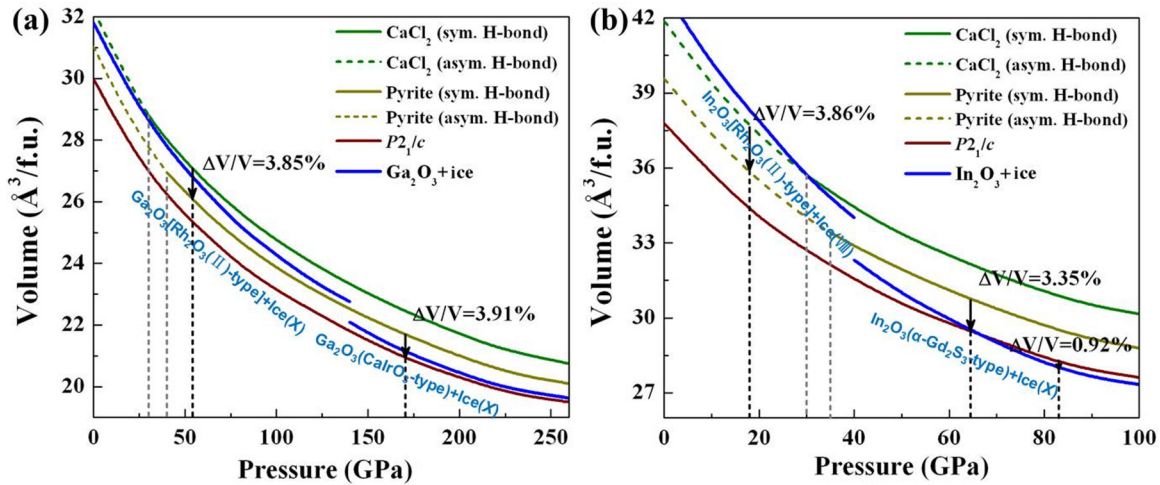
FIG. 10. Equations of state of the CaCl$_2$-, pyrite-, and monoclinic-type phases of GaOOH (a) and InOOH (b), as well as Ga$_2$O$_3$ + ice and In$_2$O$_3$ + ice. Solid and dashed lines indicate the symmetric and asymmetric hydrogen bonded structures, respectively. Vertical lines and arrows indicate transition pressures and are labeled with calculated volume collapse.

hydrous phase, with mobile protons diffusing through the Al-O lattice. Such a phase would compete with superionic ice phases, and accurate calculations of thermodynamic potentials at finite temperatures are necessary to establish their relative free energies [57].

In the solid state, the occurrence of the $P2_1/c$ phase marks a break from symmetric, linear hydrogen bonds, as more compact packing can be achieved with asymmetric and bent hydrogen bonds. At the same time, this is the first structure that increases the metal coordination to more than six, as each Al cation is coordinated to seven oxygen atoms. It represents, unlike, for instance, the ice-X to ice-$Pbcm$ transition, a nontrivial structural deviation from the pyrite structure type. Electronically, AlOOH remains a large-gap insulator dominated by ionic interactions up to the highest pressures. The new high-pressure structure of AlOOH is quite universal: it is found, in agreement with the homologue role, to be stable in the high-pressure phase diagrams of both GaOOH and InOOH: above 171 GPa for the former and in the more accessible range 65–77 GPa for the latter. The presence of

the new phase shifts the decomposition reaction of InOOH into In$_2$O$_3$ and ice upward by about 12 GPa while preventing decomposition of GaOOH up to the highest pressures studied.

[1] M. M. Hirschmann, Annu. Rev. Earth Planet. Sci. **34**, 629 (2006).

[2] J. R. Smyth and S. D. Jacobsen, Am. Geophys. Union **168**, 1 (2006).

[3] M. J. Drake and K. Righter, Nature **416**, 39 (2002).

[4] B. J. Wood, Science. **268**, 74 (1995).

[5] E. Stolper, Geochim. Cosmochim. Acta **46**, 2609 (1982).

[6] Q. Williams and R. J. Hemley, Annu. Rev. Earth Planet. Sci. **29**, 365 (2001).

[7] D. G. Pearson, F. E. Brenker, F. Nestola, J. McNeill, L. Nasdala, M. T. Hutchison, S. Matveev, K. Mather, G. Silversmit, S. Schmitz, B. Vekemans, and L. Vincze, Nature **507**, 221 (2014).

[8] B. Schmandt, S. D. Jacobsen, T. W. Becker, Z. Liu, and K. G. Dueker, Science **344**, 1265 (2014).

[9] T. Guillot, Science **286**, 72 (1999).

[10] R. J. Angel, D. J. Frost, N. L. Ross, and R. Hemley, Phys. Earth **127**, 181 (2001).

[11] S. Ono, Contrib Mineral Petrol. **137**, 83 (1999).

[12] M. W. Schmidt, L. W. Finger, R. J. Angel, and R. E. Dinnebier, Am. Mineral. **83**, 881 (1998).

[13] R. A. Eggleton, J. N. Boland, and A. E. Ringwood, Geochem. J. **12**, 191 (1978).

[14] B. Wunder, D. C. Rubie, C. R. Ross, O. Medenbach, F. Seifert, and W. Schreyer, Am. Mineral. **78**, 285 (1993).

[15] A. Suzuki, E. Ohtani, and A. Sano, EOS Trans. **82**, S409 (2001).

[16] J. Tsuchiya, Geophys. Res. Lett. **40**, 4570 (2013).

[17] A. Sano, E. Ohtani, T. Kubo, and K. Funakoshi, J. Phys. Chem. Solids **65**, 1547 (2004).

[18] J. Tsuchiya, T. Tsuchiya, and S. Tsuneyuki, Am. Mineral. **90**, 44 (2005).

[19] J. Tsuchiya, T. Tsuchiya, S. Tsuneyuki, and T. Yamanaka, Geophys. Res. Lett. **29**, 19 (2002).

[20] M. Nishi, T. Irifune, J. Tsuchiya, Y. Tange, Y. Nishihara, K. Fujino, and Y. Higo, Nat. Geosci. **7**, 224 (2014).

[21] A. Suzuki, E. Ohtani, and T. Kamada, Phys. Chem. Miner. **27**, 689 (2000).

[22] E. Ohtani, M. Toma, K. Litasov, T. Kubo, and A. Suzuki, Phys. Earth Planet. Inter. **124**, 105 (2001).

[23] A. Sano, E. Ohtani, T. Kondo, N. Hirao, T. Sakai, N. Sata, Y. Ohishi, and T. Kikegawa, Geophys. Res. Lett. **35**, L03303 (2008).

[24] T. Ishikawa, J. Tsuchiya, and T. Tsuchiya, Phys. Rev. B **83**, 212101 (2011).

[25] X. Xue and M. Kanzaki, J. Phys. Chem. B **111**, 13156 (2007).

[26] N. A. Nikolaev, L. M. Lityagina, T. I. Dyuzheva, L. F. Kulikova, and N. A. Bendeliani, J. Alloys Compd. **459**, 95 (2008).

[27] A. Neuhaus, Chimia (Aarau) **18**, 93 (1964).

[28] A. Sano, T. Yagi, T. Okada, H. Gotou, E. Ohtani, J. Tsuchiya, and T. Kikegawa, J. Miner. Pet. **103**, 152 (2008).

[29] J. Tsuchiya, T. Tsuchiya, A. Sano, and E. Ohtani, J. Miner. Pet. Sci. **103**, 116 (2008).

[30] Y. Wang, J. Lv, L. Zhu, and Y. Ma, Phys. Rev. B **82**, 094116 (2010).

[31] Y. Wang, J. Lv, L. Zhu, and Y. Ma, Comput. Phys. Comm. **183**, 2063 (2012).

[32] L. Zhu, H. Wang, Y. Wang, J. Lv, Y. Ma, Q. Cui, Y. Ma, and G. Zou, Phys. Rev. Lett. **106**, 145501 (2011).

[33] J. Lv, Y. Wang, L. Zhu, and Y. Ma, Phys. Rev. Lett. **106**, 015503 (2011).

[34] Y. Wang, H. Liu, J. Lv, L. Zhu, H. Wang, and Y. Ma, Nat. Comm. **2**, 563 (2011).

[35] X. Zhong, Y. Wang, F. Peng, H. Liu, H. Wang, and Y. Ma, Chem. Sci. **5**, 1 (2014).

[36] X. Zhong, J. Wang, S. Zhang, G. Yang, and Y. Wang, RSC Adv. **5**, 54253 (2015).

[37] A. Hermann and M. Mookherjee, Proc. Natl. Acad. Sci. **113**, 13971 (2016).

[38] P. E. Blöchl, Phys. Rev. B **50**, 17953 (1994).

[39] G. Kresse and D. Joubert, Phys. Rev. B **59**, 1758 (1999).

[40] Y. Wang and J. P. Perdew, Phys. Rev. B **43**, 8911 (1991).

[41] G. Kresse and J. Furthmüller, Phys. Rev. B **54**, 11169 (1996).

[42] C. Thierfelder, A. Hermann, P. Schwerdtfeger, and W. G. Schmidt, Phys. Rev. B **74**, 045422 (2006).

[43] See Supplemental Material at http://link.aps.org/supplemental/10.1103/PhysRevB.94.224110 for LDA results.

[44] H. J. Monkhorst and J. D. Pack, Phys. Rev. B **13**, 5188 (1976).

[45] A. Togo, F. Oba, and I. Tanaka, Phys. Rev. B **78**, 134106 (2008).

[46] J. Tsuchiya and T. Tsuchiya, Phys. Rev. B **83**, 054115 (2011).

[47] K. Umemoto and R. M. Wentzcovitch, Proc. Natl. Acad. Sci. **105**, 6526 (2008).

[48] M. Benoit, M. Bernasconi, P. Focher, and M. Parrinello, Phys. Rev. Lett. **76**, 2934 (1996).

[49] B. Militzer and H. F. Wilson, Phys. Rev. Lett. **105**, 195701 (2010).

[50] C. J. Pickard, M. Martinez-Canales, and R. J. Needs, Phys. Rev. Lett. **110**, 245701 (2013).

[51] A. Hermann, N. W. Ashcroft, and R. Hoffmann, Proc. Natl. Acad. Sci. **109**, 745 (2012).

[52] A. Hermann, N. W. Ashcroft, and R. Hoffmann, Phys. Rev. B **88**, 214113 (2013).

[53] P. Giannozzi, S. de Gironcoli, P. Pavone, and S. Baroni, Phys. Rev. B **43**, 7231 (1991).

[54] T. Duffy, N. Madhusudhan, and K. K. M. Lee, Treatise Geophys. (2nd ed.) **2**, 149 (2015).

[55] F. W. Wagner, N. Tosi, F. Sohl, H. Rauer, and T. Spohn, Astron. Astrophys. **541**, 1 (2012).

[56] J. Sun, B. K. Clark, S. Torquato, and R. Car, Nat. Comm. **6**, 8156 (2015).

[57] M. French, M. P. Desjarlais, and R. Redmer, Phys. Rev. E **93**, 022140 (2016).

[58] R. F. W. Bader, *Encyclopedia of Computational Chemistry* (John Wiley & Sons, Chichester, UK, 2002).

[59] A. D. Becke and K. E. Edgecombe, J. Chem. Phys. **92**, 5397 (1990).

[60] C. Lee, D. Vanderbilt, K. Laasonen, R. Car, and M. Parrinello, Phys. Rev. Lett. **69**, 462 (1992).

[61] A. Polian and M. Grimsditch, Phys. Rev. Lett. **52**, 1312 (1984).

[62] T. Tsuchiya, H. Yusa, and J. Tsuchiya, Phys. Rev. B **76**, 174108 (2007).

[63] H. Yusa, T. Tsuchiya, N. Sata, and Y. Ohishi, Phys. Rev. B **77**, 064107 (2008).

[64] H. Yusa, T. Tsuchiya, J. Tsuchiya, N. Sata, and Y. Ohishi, Phys. Rev. B **78**, 092107 (2008).